Analysis of Ride-Through Capability of Unidirectional-Current MMC with Arm Current Unidirectionality Disrupted

Zhengxuan Li, Qiang Song, *Senior Member, IEEE*, Biao Zhao, *Senior Member, IEEE*, Zhanqing Yu, *Member, IEEE*, Rong Zeng, *Senior Member, IEEE*, and Bin Cui, *Member, IEEE*

***Abstract*—Unidirectional-current full-bridge submodule (UC-FBSM) based modular multilevel converter (UC-FB-MMC) has high power-density, dc fault-clearing capability and dynamic dc voltage adjustability, and is therefore suitable for many new dc applications. The normal operation of UC-FB-MMC requires the arm currents being always positive. This requirement can be met in steady states by designing a sufficiently high ac voltage to decrease the ac components of the arm currents. However, some transient states may cause the arm currents to reach 0 and tend to be negative and cause the UC-FB-MMC to enter an abnormal state with non-positive arm currents. The feasibility of UC-FB-MMCs in practical applications is impacted by whether or not the UC-FB-MMCs can ride through these states. This article first analyzes the current paths and intuitively verifies that the ac- and dc-side currents are not interrupted in the states with non-positive arm currents. Then, the mathematical models of a single arm with non-positive current reveals that the ac- and dc-side currents are still under control, but the control effects become poor. After that, a modified controller is proposed to enhance the control effects. Simulation and experimental results verify the analysis.**

***Index Terms*—Current control, open-arm state, unidirectional-current full-bridge modular multilevel converter (UC-FB-MMC), unidirectional arm current.**

I. Introduction

MODULAR multilevel converters (MMCs) based on half-bridge submodule (HBSM) (HB-MMC) have been widely applied in existing high-voltage dc (HVDC) projects [1]. With the development of converter and dc techniques, many applications that require the MMCs to have high power density and special functions have emerged, including the dc fault clearing capability [2] and dynamic dc voltage adjustability [3], [4], [5]. However, none of these objectives can be realized by the HB-MMCs. For one thing, large capacitors used in the HB-MMCs result in large footprints and low power-density [6]. For the other, the HB-MMCs can neither clear the dc faults nor dynamically adjust the dc voltages because the HBSMs can only output 0 and positive voltages. As such, the emerging applications are calling for new submodule topologies.

Full-bridge submodule (FBSM), which can output an additional negative voltage level compared with the HBSM, was originally proposed to clear the dc faults [2]. Recent studies have noticed that using the negative voltage states of the FBSMs, the FBSM-based MMCs (FB-MMCs) can widely adjust the dc voltage without affecting the ac voltage output [7], [8], [9]. It is also revealed that the negative voltage states can help increase the modulation index [10], [11], [12], thereby reducing the submodule capacitance effectively [10], [11], [12]. Given these advantages, the FB-MMCs are very suitable for the abovementioned emerging applications. However, compared with the HB-MMCs, the FB-MMCs demand excessive extra semiconductors [12], resulting in high cost and power losses, which restrict the practical applications.

In many dc applications, the power is transmitted unidirectionally. Considering these applications, a variant of FBSM named unidirectional-current FBSM (UC-FBSM) was proposed in [13] and [14] to reduce the semiconductor usage. The normal operation of the UC-FBSM-based MMC (UC-FB-MMC) requires the arm currents being unidirectional. To meet this requirement, a discontinuous arm current control was proposed in [13] and [14], but the current references are quite different from the conventional MMCs, and the conventional MMC control cannot be easily implemented to the UC-FB-MMC. To cope with this problem, Yu et al. [15] proposed to design an increased ac voltage to decrease the ac components in the arm currents, thereby creating the unidirectional arm currents using the conventional control strategies. As such, the dc components can help create the unidirectional arm currents. In [16], an active circulating current injection was proposed to reduce the ac voltage requirement by 1/3. Deng et al. [17] proposed a control strategy for the hybrid dc system based on line commuted converter (LCC) and UC-FB-MMC. A dynamic braking resistor circuit based on UC-FBSM was proposed in [18]. In [19], by combining two UC-FBSMs, a unidirectional-current clamp-double submodule was proposed to further reduce the quantities of semiconductor devices. The UC-FB-MMC inherits the advantages of FB-MMC: The dc fault clearing capability

Manuscript received 5 January 2024; revised 7 March 2024; accepted 13 April 2024. Date of publication 23 April 2024; date of current version 20 June 2024. This work was supported in part by the National Key R&D Program of China under Grant 2022YFB2405300 and in part by the National Natural Science Foundation of China under Grant 51977119. Recommended for publication by Associate Editor F. Freijedo. *(Corresponding author: Qiang Song.)*

The authors are with the Department of Electrical Engineering, Tsinghua University, Beijing 100084, China (e-mail: zx-li18@tsinghua.org.cn; songqiang@tsinghua.edu.cn; zhao-biao@tsinghua.edu.cn; yzq@tsinghua.edu.cn; zengrong@tsinghua.edu.cn; cuibin@tsinghua.edu.cn).

Color versions of one or more figures in this article are available at https://doi.org/10.1109/TPEL.2024.3392723.

Digital Object Identifier 10.1109/TPEL.2024.3392723

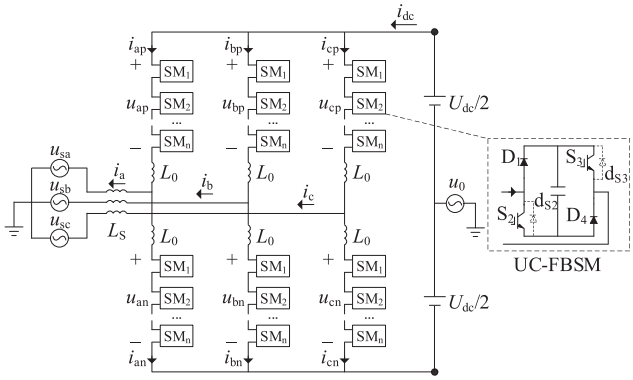

Fig. 1. Topology of UC-FB-MMC and UC-FBSM.

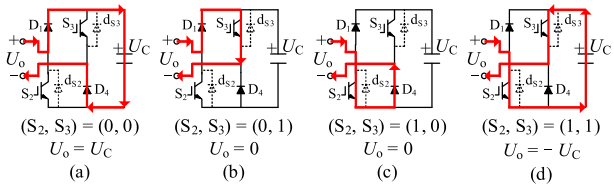

Fig. 2. Switch states, current paths, and output voltages of UC-FBSM with positive currents.

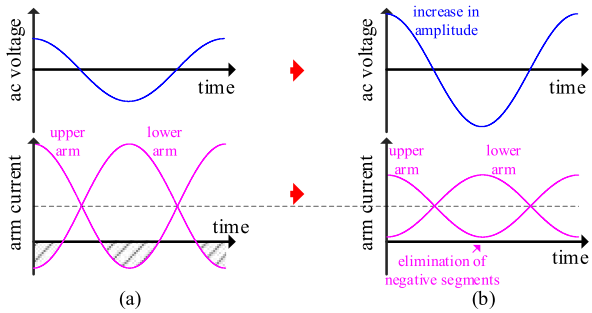

Fig. 3. Basic principle of creating unidirectional arm currents. (a) Conventional ac voltage design and bidirectional arm currents. (b) Increased ac voltage and unidirectional arm currents.

enables the UC-FB-MMC to be suitable for the long-distance overhead line-based HVDC systems [16]; the negative voltage capability of the UC-FBSM can reduce the converter volume and increase the power density [20], and enables the UC-FB-MMCs to widely adjust the dc voltage [3], which is very important in the ultrahigh voltage dc systems.

While the exiting studies indicate that the UC-FB-MMC can operate well by creating the unidirectional arm currents in steady states, it is still possible that some arm currents may lose unidirectionality because of external disturbance. For instance, if faults occur in the ac or dc systems, the ac or dc components of the arm currents may be affected, thus causing some arm currents to lose unidirectionality. Also, if the current references change rapidly, the errors between the reference and the actual values may also cause the arm currents to lose unidirectionality temporarily.

While there has hitherto never been such a report that a transient loss of unidirectionality of arm currents causes severe faults of UC-FB-MMCs mentioned in any study, yet whether the UC-FB-MMC can continue operating and ride through the entire transient state with non-unidirectional arm currents is still a key issue that impacts on whether the UC-FB-MMC is feasible in practical applications. This article conducts research on the operation characteristics of the UC-FB-MMC when some arm currents lose unidirectionality.

The rest of this article is organized as follows. The arm current states of the UC-FB-MMC are analyzed in Section II, and it is found that even some arm currents cannot maintain unidirectional, the ac and dc currents will not be interrupted because their paths are still guaranteed, and thus, severe faults will not occur. Then, a mathematical model is deduced in Section III to analyze the controllability of the ac- and dc-side currents when an arm current loses unidirectionality, and a modified decoupled controller is proposed in Section IV to enhance the current control effects. Simulation and experimental results are given in Section V. Finally, Section VI concludes this article.

II. Current Path Analysis for UC-FB-MMC With Non-Positive Arm Currents

Fig. 1 shows the topologies of the UC-FB-MMC and UC-FBSM. The switching devices and diodes S_2, S_3, D_1, and D_4 are for the arm currents during normal operation. Only if the MMC is pre-charged from its ac side are the diodes d_{S2} and d_{S3} necessary. Considering that some types of power electronic switching devices are integrated with diodes while others are not, this article draws d_{S2} and d_{S3} separately using dashed lines. The positive direction of the arm and submodule currents are defined using the arrows in Fig. 1. Fig. 2 shows that the UC-FBSM can output positive, zero, and negative voltage levels with a positive current. Therefore, all the arm currents in normal operation must always be positive. It is pointed out in [15] and [16] that the always-positive arm currents in steady states can be created by designing a sufficiently high ac voltage, because increasing the ac voltage can reduce the fundamental components in the arm currents, as shown in Fig. 3.

Although the special design of the ac voltage can guarantee steady-state positive arm currents, disturbance in transient states may cause some arm currents to reach 0 and tend to be negative. These transient states may include but are not limited to reactive power increase, occurrence of faults and rapid changes of current references. Different from other MMC topologies, if an arm current of the UC-FB-MMC tends to be negative, all the submodule capacitors are automatically inserted negatively into the circuit regardless of the pulse signals of the switching devices, thereby generating a large negative voltage, as shown in Fig. 4(a). As shown in Fig. 4(b), the external circuit is equivalent to a voltage source with resistor. If the arm voltage output is negatively greater than that of the external source, then the diode suddenly enters the cut-off state and blocks the current. If the voltage of the external source is negatively greater than the arm output voltage, then the flowing current will charge the capacitors, and finally, the negative voltage generated by the capacitors will be so large that it blocks the diode and the current. For either case,

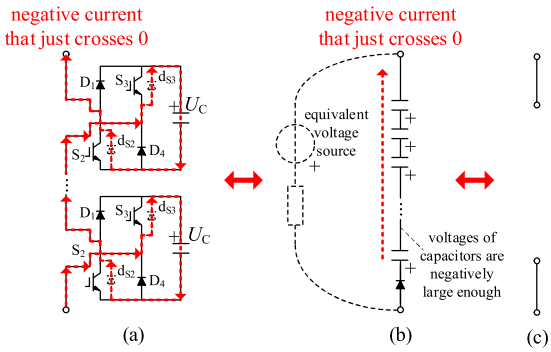

Fig. 4. (a) Current path, (b) and (c) equivalent circuits when arm current just crosses 0 from positive to negative.

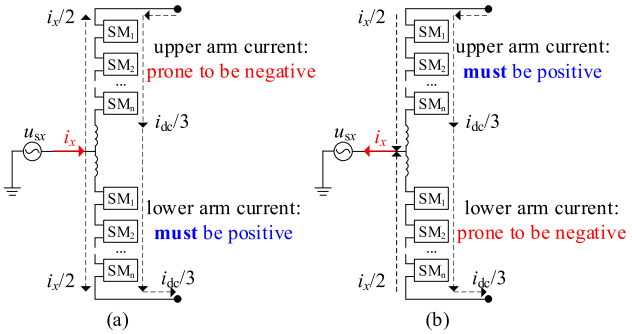

Fig. 5. Arm current conditions when ac-side current flows (a) into and (b) out of the converter.

the negative current will be finally clamped to approximately 0. As such, the arm is approximately equivalent to an open circuit, as shown in Fig. 4(c).

In fact, whether an arm current is prone to be negative is closely related to the direction of the ac-side current. Taking a phase leg as an example, Fig. 5 compares the arm current conditions when the ac-side current flows into and out of the converter. Specifically, as show in Fig. 5(a), when the ac-side current flows into the converter, it brings a negative component to the upper arm current and a positive component to the lower arm current. As a result, the upper arm current is prone to be negative while the lower arm current must be positive. By comparison, as shown in Fig. 5(b), when the ac-side current flows out of the converter, it brings a negative component to the lower arm current and a positive component to the upper arm current. As such, the lower arm current is prone to be negative while the upper arm current must be positive. To sum up, at least one of the two converter arms in a phase leg must have the positive current and be in operation. Whether the other arm is in operation or open is determined by its current condition: If the arm current is positive, then the arm is also in operation; if the arm current tends to be negative, then the arm is equivalent to an open circuit.

In a UC-FB-MMC, if all the arm currents are positive, then all the converter arms operate normally, and thus, this article defines this state as *the normal state*. By comparison, the states where some converter arms are open due to the negative current tendencies are defined as *the open-arm states*. Based on the analysis of a phase leg in Fig. 5, there are at most three open arms in a UC-FB-MMC even in the worst case. Therefore, the open-arm states are divided into single-, double-, and triple-open-arm states based on the quantity of open arms, and all the possible open-arm states are given in Tables I–III. For intuitive illustration, Fig. 6 shows the current paths of the single-, double- and triple-open-arm states, where the condition that i_a flows into and i_b and i_c flow out of the converter is taken as an example. Given that the double-open-arm states are also related to the current magnitudes, Fig. 6(b) assumes that $|i_a| > |i_b| > |i_c|$. The directions of the arrows in Fig. 6 are the reference directions of the currents, while the greater-than and lower-than signs indicate the actual directions. Referring to Fig. 6 and Tables I–III, the open-arm states are explained as follows.

1) *Single-Open-Arm State*: With one open arm.
2) *Double-Open-Arm State*: With two open arms in DIFFERENT phases.
3) *Triple-Open-Arm State*: With three open arms in three DIFFERENT phases. Due to the different directions of the three ac-side currents, the operating arms must contain at least one upper and one lower arms.

TABLE I
SUMMARY OF ALL POSSIBLE SINGLE-OPEN-ARM STATES

Open arms*	Operating arms	Conditions
an	ap, bp, bn, cp, cn	$i_a > 0, i_b < 0, i_c < 0$
cp	ap, an, bp, bn, cn	$i_a > 0, i_b > 0, i_c < 0$
bn	ap, an, bp, cp, cn	$i_a < 0, i_b > 0, i_c < 0$
ap	an, bp, bn, cp, cn	$i_a < 0, i_b > 0, i_c > 0$, Fig. 6(a)
cn	ap, an, bp, bn, cp	$i_a < 0, i_b < 0, i_c > 0$
bp	ap, an, bn, cp, cn	$i_a > 0, i_b < 0, i_c > 0$

* a, b, and c denote the three phases, and p and n denote the upper and lower arms, respectively.

TABLE II
SUMMARY OF ALL POSSIBLE DOUBLE-OPEN-ARM STATES

Open arms	Operating arms	Conditions
an, cp	ap, bp, bn, cn	$i_a > 0, i_b < 0, i_c < 0, \|i_a\| > \|i_c\| > \|i_b\|$ or $i_a > 0, i_b > 0, i_c < 0, \|i_c\| > \|i_a\| > \|i_b\|$
bn, cp	ap, an, bp, cn	$i_a > 0, i_b > 0, i_c < 0, \|i_c\| > \|i_b\| > \|i_a\|$ or $i_a < 0, i_b > 0, i_c < 0, \|i_b\| > \|i_c\| > \|i_a\|$
ap, bn	an, bp, cp, cn	$i_a < 0, i_b > 0, i_c < 0, \|i_b\| > \|i_a\| > \|i_c\|$or $i_a < 0, i_b > 0, i_c > 0, \|i_a\| > \|i_b\| > \|i_c\|$, Fig. 6(b)
ap, cn	an, bp, bn, cp	$i_a < 0, i_b > 0, i_c > 0, \|i_a\| > \|i_c\| > \|i_b\|$ or $i_a < 0, i_b < 0, i_c > 0, \|i_c\| > \|i_a\| > \|i_b\|$
bp, cn	ap, an, bn, cp	$i_a < 0, i_b < 0, i_c > 0, \|i_c\| > \|i_b\| > \|i_a\|$or $i_a > 0, i_b < 0, i_c > 0, \|i_b\| > \|i_c\| > \|i_a\|$
an, bp	ap, bn, cp, cn	$i_a > 0, i_b < 0, i_c > 0, \|i_b\| > \|i_a\| > \|i_c\|$or $i_a > 0, i_b < 0, i_c < 0, \|i_a\| > \|i_b\| > \|i_c\|$

TABLE III
SUMMARY OF ALL POSSIBLE TRIPLE-OPEN-ARM STATES

Open arms	Operating arms	Conditions
an, bp, cp	ap, bn, cn	$i_a > 0, i_b < 0, i_c < 0$
an, bn, cp	ap, bp, cn	$i_a > 0, i_b > 0, i_c < 0$
ap, bn, cp	an, bp, cn	$i_a < 0, i_b > 0, i_c < 0$
ap, bn, cn	an, bp, cp	$i_a < 0, i_b > 0, i_c > 0$, Fig. 6(c)
ap, bp, cn	an, bn, cp	$i_a < 0, i_b < 0, i_c > 0$
an, bp, cn	ap, bn, cp	$i_a > 0, i_b < 0, i_c > 0$

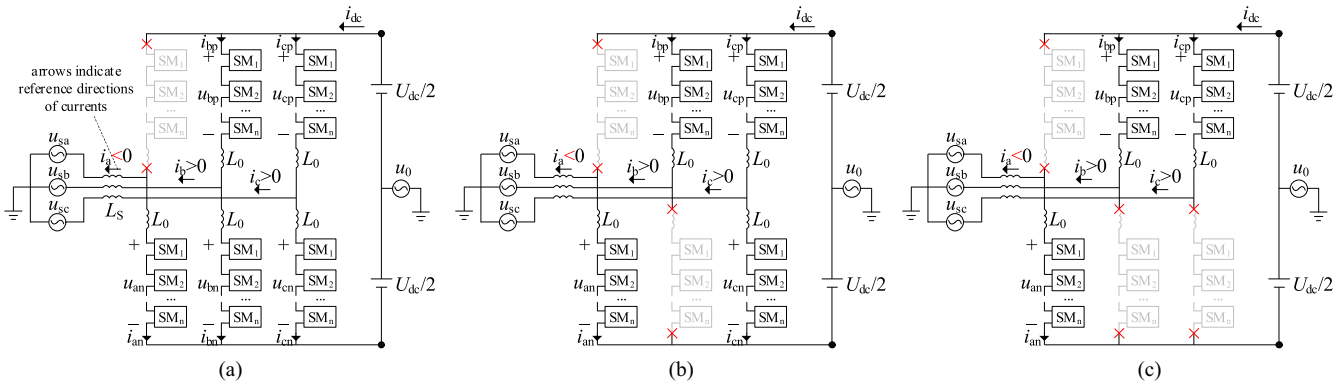

Fig. 6. Possible current path examples of (a) single, (b) double, and (c) triple open arms. Current direction conditions: $i_{\rm a}$ flows into the converter and $i_{\rm b}$ and $i_{\rm c}$ flow out of the converter. Current magnitude condition for subfigure (b): $|i_{\rm a}| > |i_{\rm b}| > |i_{\rm c}|$.

As shown by the examples in Fig. 6, given that each phase has at least one operating arm, the ac-side currents can flow. Given that at least one upper arm and one lower arm are in operation, the dc-side current can also flow. Therefore, in all these 18 conditions, the ac- and dc-side current paths still exist, and the ac- and dc-side currents will not be interrupted. This indicates that temporary open-arm states (regardless of single-, double-, and triple-ones) may hardly develop into serious faults, and the MMC can restore into the normal state once the external disturbance, which causes the open-arm states, disappears.

III. Mathematical Model of UC-FB-MMC in Single-Open-Arm States

According to Section II, if any arm current has a negative tendency, then the UC-FB-MMC shifts from the normal to the open-arm states, but the ac- and dc-side currents can still flow, which indicates that temporary open-arm states may hardly develop into serious faults. However, from the perspective of operational reliability, the analyses based on mathematical models are still essential. Given that the single-, double-, and triple-open-arm states have a developing relationship, it is reasonable to assume that if the MMC is well-controlled in the single-open-arm states, the double- and triple-open-arm states might be avoided. Therefore, this section deduces the mathematical model of the UC-FB-MMC in the single-open-arm states, and analyzes the current control effects.

Section III-A briefly summarizes the normal-state model and control diagrams according the existing studies [21], [22]. Then, Section III-B takes the single-open-arm states as examples and analyzes the control effects of the existing controller. It is concluded that the ac- and dc-side currents are still under control, but the coupling between them exists, which affects the control effects.

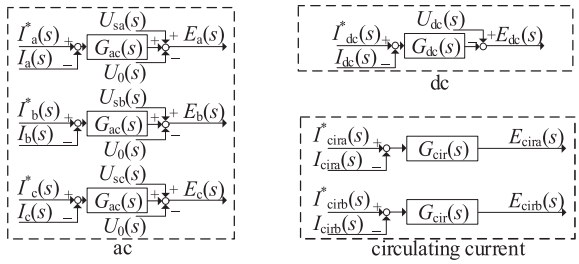

Fig. 7. Control diagram of UC-FB-MMCs.

A. Normal-State Model and Controller Diagrams

The voltage equations can be obtained according to Fig. 1. To facilitate the following analysis, the obtained equations are illustrated in the complex frequency domain as (1) at the bottom of this page, where the subscripts a, b, and c denote the three phases, and p and n denote the upper and lower arms, respectively; s denotes the complex frequency; $I_{\rm ap}(s)$, $I_{\rm bp}(s)$, $I_{\rm cp}(s)$, $I_{\rm an}(s)$, $I_{\rm bn}(s)$, and $I_{\rm cn}(s)$ are the arm currents; $U_{\rm ap}(s)$, $U_{\rm bp}(s)$, $U_{\rm cp}(s)$, $U_{\rm an}(s)$, $U_{\rm bn}(s)$, and $U_{\rm cn}(s)$ are the arm voltages; $U_{\rm sa}(s)$, $U_{\rm sb}(s)$, $U_{\rm sc}(s)$ are the system ac voltages; $U_{\rm dc}(s)$

$$
\begin{cases}
(L_0+2L_{\rm S})\,sI_{\rm ap}(s) = -\left(1+\frac{L_{\rm S}}{L_0}\right)U_{\rm ap}(s) - \frac{L_{\rm S}}{L_0}U_{\rm an}(s) - U_{\rm sa}(s) + \left(\frac{1}{2}+\frac{L_{\rm S}}{L_0}\right)U_{\rm dc}(s) + U_0(s)\\
(L_0+2L_{\rm S})\,sI_{\rm bp}(s) = -\left(1+\frac{L_{\rm S}}{L_0}\right)U_{\rm bp}(s) - \frac{L_{\rm S}}{L_0}U_{\rm bn}(s) - U_{\rm sb}(s) + \left(\frac{1}{2}+\frac{L_{\rm S}}{L_0}\right)U_{\rm dc}(s) + U_0(s)\\
(L_0+2L_{\rm S})\,sI_{\rm cp}(s) = -\left(1+\frac{L_{\rm S}}{L_0}\right)U_{\rm cp}(s) - \frac{L_{\rm S}}{L_0}U_{\rm cn}(s) - U_{\rm sc}(s) + \left(\frac{1}{2}+\frac{L_{\rm S}}{L_0}\right)U_{\rm dc}(s) + U_0(s)\\
(L_0+2L_{\rm S})\,sI_{\rm an}(s) = -\frac{L_{\rm S}}{L_0}U_{\rm ap}(s) - \left(1+\frac{L_{\rm S}}{L_0}\right)U_{\rm an}(s) + U_{\rm sa}(s) + \left(\frac{1}{2}+\frac{L_{\rm S}}{L_0}\right)U_{\rm dc}(s) - U_0(s)\\
(L_0+2L_{\rm S})\,sI_{\rm bn}(s) = -\frac{L_{\rm S}}{L_0}U_{\rm bp}(s) - \left(1+\frac{L_{\rm S}}{L_0}\right)U_{\rm bn}(s) + U_{\rm sb}(s) + \left(\frac{1}{2}+\frac{L_{\rm S}}{L_0}\right)U_{\rm dc}(s) - U_0(s)\\
(L_0+2L_{\rm S})\,sI_{\rm cn}(s) = -\frac{L_{\rm S}}{L_0}U_{\rm cp}(s) - \left(1+\frac{L_{\rm S}}{L_0}\right)U_{\rm cn}(s) + U_{\rm sc}(s) + \left(\frac{1}{2}+\frac{L_{\rm S}}{L_0}\right)U_{\rm dc}(s) - U_0(s)
\end{cases}
\tag{1}
$$

is the dc voltage; $U_0(s)$ is the equivalent voltage between the ac and dc neutral points; and L_0 and L_S are the arm and ac inductances, respectively.

The ac- and dc-side currents, and the circulating currents can be calculated using the arm currents [21], expressed as

$$\begin{bmatrix} I_a(s) \\ I_b(s) \\ I_c(s) \\ I_{dc}(s) \\ I_{cira}(s) \\ I_{cirb}(s) \end{bmatrix} = \begin{bmatrix} 1 & 0 & 0 & -1 & 0 & 0 \\ 0 & 1 & 0 & 0 & -1 & 0 \\ 0 & 0 & 1 & 0 & 0 & -1 \\ 1/2 & 1/2 & 1/2 & 1/2 & 1/2 & 1/2 \\ 1/3 & -1/6 & -1/6 & 1/3 & -1/6 & -1/6 \\ -1/6 & 1/3 & -1/6 & -1/6 & 1/3 & -1/6 \end{bmatrix} \times \begin{bmatrix} I_{ap}(s) \\ I_{bp}(s) \\ I_{cp}(s) \\ I_{an}(s) \\ I_{bn}(s) \\ I_{cn}(s) \end{bmatrix}. \tag{2}$$

To simplify the model, the intermediate controllable voltages (ICVs) are defined in [21], expressed as

$$\begin{bmatrix} E_a(s) \\ E_b(s) \\ E_c(s) \\ E_{dc}(s) \\ E_{cira}(s) \\ E_{cira}(s) \end{bmatrix} = \begin{bmatrix} -1/2 & 0 & 0 & 1/2 & 0 & 0 \\ 0 & -1/2 & 0 & 0 & 1/2 & 0 \\ 0 & 0 & -1/2 & 0 & 0 & 1/2 \\ 1/3 & 1/3 & 1/3 & 1/3 & 1/3 & 1/3 \\ 1 & -1/2 & -1/2 & 1 & -1/2 & -1/2 \\ -1/2 & 1 & -1/2 & -1/2 & 1 & -1/2 \end{bmatrix} \times \begin{bmatrix} U_{ap}(s) \\ U_{bp}(s) \\ U_{cp}(s) \\ U_{an}(s) \\ U_{bn}(s) \\ U_{cn}(s) \end{bmatrix}. \tag{3}$$

Substituting (2) and (3) into (1) shown at the bottom of the previous page, yields the decoupled mathematical model as follows [21]:

$$s \begin{bmatrix} (L_0/2 + L_S) I_a(s) \\ (L_0/2 + L_S) I_b(s) \\ (L_0/2 + L_S) I_c(s) \\ 2L_0/3 I_{dc}(s) \\ 3L_0 I_{cira}(s) \\ 3L_0 I_{cirb}(s) \end{bmatrix} = \begin{bmatrix} E_a(s) \\ E_b(s) \\ E_c(s) \\ -E_{dc}(s) \\ E_{cira}(s) \\ E_{cirb}(s) \end{bmatrix} + \begin{bmatrix} -1 & 0 & 0 & 0 & 1 \\ 0 & -1 & 0 & 0 & 1 \\ 0 & 0 & -1 & 0 & 1 \\ 0 & 0 & 0 & 1 & 0 \\ 0 & 0 & 0 & 0 & 0 \\ 0 & 0 & 0 & 0 & 0 \end{bmatrix} \times \begin{bmatrix} U_{sa}(s) \\ U_{sb}(s) \\ U_{sc}(s) \\ U_{dc}(s) \\ U_0(s) \end{bmatrix}. \tag{4}$$

The controllers shown in Fig. 7 are designed based on (4) [21]. After the ICVs are obtained, the arm voltage references are generated using

$$\begin{bmatrix} U^*_{ap}(s) \\ U^*_{bp}(s) \\ U^*_{cp}(s) \\ U^*_{an}(s) \\ U^*_{bn}(s) \\ U^*_{cn}(s) \end{bmatrix} = \begin{bmatrix} -1 & 0 & 0 & 1/2 & -1/3 & 0 \\ 0 & -1 & 0 & 1/2 & 0 & -1/3 \\ 0 & 0 & -1 & 1/2 & 1/3 & 1/3 \\ 1 & 0 & 0 & 1/2 & -1/3 & 0 \\ 0 & 1 & 0 & 1/2 & 0 & -1/3 \\ 0 & 0 & 1 & 1/2 & 1/3 & 1/3 \end{bmatrix} \times \begin{bmatrix} E_a(s) \\ E_b(s) \\ E_c(s) \\ E_{dc}(s) \\ E_{cira}(s) \\ E_{cirb}(s) \end{bmatrix}. \tag{5}$$

To simplify the deduction, this article chooses the *abc* frame for the ac controllers in Fig. 7. $G_{ac}(s)$, $G_{dc}(s)$, and $G_{cir}(s)$ denote the open-loop transfer functions of the ac, dc and circulating current control loops, respectively; and $I^*_a(s), I^*_b(s), I^*_c(s), I^*_{dc}(s), I^*_{cira}(s)$, and $I^*_{cirb}(s)$ denote the current references. Given that the design of the controllers is not the core of this article, the expressions of $G_{ac}(s)$, $G_{dc}(s)$, and $G_{cir}(s)$ are not specified. Based on Fig. 7, the ICVs are obtained as

$$\begin{bmatrix} E_a(s) \\ E_b(s) \\ E_c(s) \\ E_{dc}(s) \\ E_{cira}(s) \\ E_{cirb}(s) \end{bmatrix} = \begin{bmatrix} G_{ac}(s)\left(I^*_a(s) - I_a(s)\right) + U_{sa}(s) - U_0(s) \\ G_{ac}(s)\left(I^*_b(s) - I_b(s)\right) + U_{sb}(s) - U_0(s) \\ G_{ac}(s)\left(I^*_c(s) - I_c(s)\right) + U_{sc}(s) - U_0(s) \\ -G_{dc}(s)\left(I^*_{dc}(s) - I_{dc}(s)\right) + U_{dc}(s) \\ G_{cir}(s)\left(I^*_{cira}(s) - I_{cira}(s)\right) \\ G_{cir}(s)\left(I^*_{cirb}(s) - I_{cirb}(s)\right) \end{bmatrix}. \tag{6}$$

Substituting (6) into (4) yields the relationship between the currents and their references as

$$s \begin{bmatrix} (L_0/2 + L_S) I_a(s) \\ (L_0/2 + L_S) I_b(s) \\ (L_0/2 + L_S) I_c(s) \\ 2L_0/3 I_{dc}(s) \\ 3L_0 I_{cira}(s) \\ 3L_0 I_{cirb}(s) \end{bmatrix} = \mathbf{C} \times \begin{bmatrix} I^*_a(s) - I_a(s) \\ I^*_b(s) - I_b(s) \\ I^*_c(s) - I_c(s) \\ I^*_{dc}(s) - I_{dc}(s) \\ I^*_{cira}(s) - I_{cira}(s) \\ I^*_{cirb}(s) - I_{cirb}(s) \end{bmatrix} \tag{7}$$

where

$$\mathbf{C} = \begin{bmatrix} G_{ac}(s) & 0 & 0 & 0 & 0 & 0 \\ 0 & G_{ac}(s) & 0 & 0 & 0 & 0 \\ 0 & 0 & G_{ac}(s) & 0 & 0 & 0 \\ 0 & 0 & 0 & G_{dc}(s) & 0 & 0 \\ 0 & 0 & 0 & 0 & G_{cir}(s) & 0 \\ 0 & 0 & 0 & 0 & 0 & G_{cir}(s) \end{bmatrix}. \tag{8}$$

Given that all the off-diagonal elements in the matrix $\mathbf{C}$ are zeros, the ac- and dc-side currents are decoupled. That is, in the normal state, the controls of ac- and dc-side currents do not interact with each other, and the currents are determined only by their respective references and controllers.

B. Analysis of Single-Open-Arm States

Section II concludes that there are totally 18 possible open-arm states that are divided into the single-, double- and triple-open-arm states. Due to limited space, this article only takes the single-open-arm states, which are the simplest conditions, as examples to present the analysis. Another issue is that there are totally six conditions of single-open-arm states, which appear in the order of ap, cn, bp, an, cp, bn, as listed in Table I. Given that the analysis is similar in the six conditions, the state where the upper arm of phase A is open is taken as an example.

Similar to the normal state, the voltage equations in complex frequency domain can be obtained according to Fig. 6(a), expressed as (9) shown at the bottom of this page, where the definitions of the variables are the same as those in (1).

Substituting (2) and (3) into (9) [except for $I_{\rm ap}(s)$ and $U_{\rm ap}(s)$], the mathematical model in the single-open-arm state becomes

$$
\begin{aligned}
&s\begin{bmatrix}(L_0/2+L_{\rm S})\,I_{\rm a}(s)\\(L_0/2+L_{\rm S})\,I_{\rm b}(s)\\(L_0/2+L_{\rm S})\,I_{\rm c}(s)\\2L_0/3I_{\rm dc}(s)\\3L_0I_{\rm cirb}(s)\end{bmatrix}\\
&=\begin{bmatrix}\frac{L_0+2L_{\rm S}}{2L_0+2L_{\rm S}} & 0 & 0 & \frac{L_0+2L_{\rm S}}{4L_0+4L_{\rm S}} & 0\\ 0 & 1 & 0 & 0 & 0\\ 0 & 0 & 1 & 0 & 0\\ -\frac{L_0}{3L_0+3L_{\rm S}} & 0 & 0 & -\frac{5L_0+4L_{\rm S}}{6L_0+6L_{\rm S}} & 0\\ \frac{L_0}{2L_0+2L_{\rm S}} & 0 & 0 & -\frac{L_0+2L_{\rm S}}{4L_0+4L_{\rm S}} & 1\end{bmatrix}\times\begin{bmatrix}E_{\rm a}(s)\\E_{\rm b}(s)\\E_{\rm c}(s)\\E_{\rm dc}(s)\\E_{\rm cirb}(s)\end{bmatrix}\\
&+\begin{bmatrix}-\frac{L_0+2L_{\rm S}}{2L_0+2L_{\rm S}} & 0 & 0 & -\frac{L_0+2L_{\rm S}}{4L_0+4L_{\rm S}} & \frac{L_0+2L_{\rm S}}{2L_0+2L_{\rm S}}\\ 0 & -1 & 0 & 0 & 1\\ 0 & 0 & -1 & 0 & 1\\ \frac{L_0}{3L_0+3L_{\rm S}} & 0 & 0 & \frac{5L_0+4L_{\rm S}}{6L_0+6L_{\rm S}} & -\frac{L_0}{3L_0+3L_{\rm S}}\\ -\frac{L_0}{2L_0+2L_{\rm S}} & 0 & 0 & \frac{L_0+2L_{\rm S}}{4L_0+4L_{\rm S}} & \frac{L_0}{2L_0+2L_{\rm S}}\end{bmatrix}\\
&\times\begin{bmatrix}U_{\rm sa}(s)\\U_{\rm sb}(s)\\U_{\rm sc}(s)\\U_{\rm dc}(s)\\U_0(s)\end{bmatrix}. \qquad (10)
\end{aligned}
$$

If the calculations of ICVs and the transformation from ICVs to the arm voltage references in the normal states [i.e., Fig. 7 and (5)] are still implemented, then substituting (6) into (10) yields the current relationships between the references and the actual values when the upper arm of phase A is open:

$$
s\begin{bmatrix}(L_0/2+L_{\rm S})\,I_{\rm a}(s)\\(L_0/2+L_{\rm S})\,I_{\rm b}(s)\\(L_0/2+L_{\rm S})\,I_{\rm c}(s)\\2L_0/3I_{\rm dc}(s)\\3L_0I_{\rm cirb}(s)\end{bmatrix}=\mathbf{C}'\times\begin{bmatrix}I^*_{\rm a}(s)-I_{\rm a}(s)\\I^*_{\rm b}(s)-I_{\rm b}(s)\\I^*_{\rm c}(s)-I_{\rm c}(s)\\I^*_{\rm dc}(s)-I_{\rm dc}(s)\\I^*_{\rm cirb}(s)-I_{\rm cirb}(s)\end{bmatrix}, \qquad (11)
$$

where $\mathbf{C}'$ is shown in (12) at the bottom of the next page.

If the calculations of ICVs and the transformation from ICVs to the arm voltage references in the normal states [i.e., Fig. 7 and (5)] are still implemented, then the mathematical model of the UC-FB-MMC in the single-open-arm state would be (11) and (12). In $\mathbf{C}'$, the diagonal elements indicate that the current references still have impact on the actual values. However, different from (8), the off-diagonal elements that exist in (12) indicate that the phase-A and dc-side currents are coupled, which will affect the control effects and cause harmonic distortions. Moreover, if the open-arm states last longer than a grid cycle, apart from phase A, the current waveforms of phases B and C will also be affected because the open arm changes its position among the six converter arms according to the current phases.

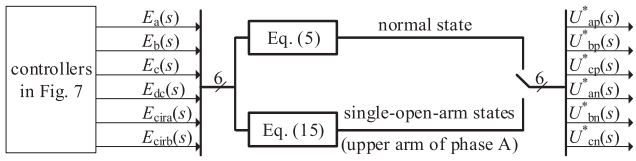

Fig. 8. Diagram of modified controller.

IV. Modified Controller of UC-FB-MMC in Single-Open-Arm States

Based on the mathematical models of the UC-FB-MMCs, the existing studies have proposed the normal-state control, including the calculations of ICVs and the transformation from the ICVs to the arm voltage references [i.e., Fig. 7 and (5)] [21]. However, based on Section III, if the normal-state control is implemented during the single-open-arm states, the control effects of the ac- and dc-side currents will become poor because of the coupling of the currents. This section proposes a modified controller to enhance the control effects, where the original ac and dc controllers shown in Fig. 7 are still used, whereas the transformation from the ICVs to the arm voltages is modified. This modification can enhance the control effects of the ac- and dc-side currents.

$$
\begin{cases}
(L_0+2L_{\rm S})\,sI_{\rm bp}(s)=-\left(1+\frac{L_{\rm S}}{L_0}\right)U_{\rm bp}(s)-\frac{L_{\rm S}}{L_0}U_{\rm bn}(s)-U_{\rm sb}(s)+\left(\frac{1}{2}+\frac{L_{\rm S}}{L_0}\right)U_{\rm dc}(s)+U_0(s)\\
(L_0+2L_{\rm S})\,sI_{\rm cp}(s)=-\left(1+\frac{L_{\rm S}}{L_0}\right)U_{\rm cp}(s)-\frac{L_{\rm S}}{L_0}U_{\rm cn}(s)-U_{\rm sc}(s)+\left(\frac{1}{2}+\frac{L_{\rm S}}{L_0}\right)U_{\rm dc}(s)+U_0(s)\\
(L_0+2L_{\rm S})\,sI_{\rm an}(s)=-\frac{L_0+2L_{\rm S}}{L_0+L_{\rm S}}U_{\rm an}(s)+\frac{L_0+2L_{\rm S}}{L_0+L_{\rm S}}U_{\rm sa}(s)+\frac{L_0+2L_{\rm S}}{2L_0+2L_{\rm S}}U_{\rm dc}(s)\\
\qquad\qquad-\frac{L_0+2L_{\rm S}}{L_0+L_{\rm S}}U_0(s)\\
(L_0+2L_{\rm S})\,sI_{\rm bn}(s)=-\frac{L_{\rm S}}{L_0}U_{\rm bp}(s)-\left(1+\frac{L_{\rm S}}{L_0}\right)U_{\rm bn}(s)+U_{\rm sb}(s)+\left(\frac{1}{2}+\frac{L_{\rm S}}{L_0}\right)U_{\rm dc}(s)-U_0(s)\\
(L_0+2L_{\rm S})\,sI_{\rm cn}(s)=-\frac{L_{\rm S}}{L_0}U_{\rm cp}(s)-\left(1+\frac{L_{\rm S}}{L_0}\right)U_{\rm cn}(s)+U_{\rm sc}(s)+\left(\frac{1}{2}+\frac{L_{\rm S}}{L_0}\right)U_{\rm dc}(s)-U_0(s)
\end{cases} \qquad (9)
$$

The state that the upper arm of phase A is open is still taken as an example. Substituting (2) into (9) yields

$$
\begin{aligned}
&s\begin{bmatrix}(L_0/2+L_S)\,I_a(s)\\(L_0/2+L_S)\,I_b(s)\\(L_0/2+L_S)\,I_c(s)\\2L_0/3I_{dc}(s)\\3L_0I_{cirb}(s)\end{bmatrix}\\
&=\begin{bmatrix}0&0&\frac{L_0+2L_S}{2L_0+2L_S}&0&0\\-1/2&0&0&1/2&0\\0&-1/2&0&0&1/2\\-\frac{1}{3}&-\frac{1}{3}&-\frac{L_0}{3L_0+3L_S}&-\frac{1}{3}&-\frac{1}{3}\\-1&\frac{1}{2}&\frac{L_0}{2L_0+2L_S}&-1&\frac{1}{2}\end{bmatrix}\times\begin{bmatrix}U_{bp}(s)\\U_{cp}(s)\\U_{an}(s)\\U_{bn}(s)\\U_{cn}(s)\end{bmatrix}\\
&+\begin{bmatrix}\frac{L_0}{2L_0+2L_S}&0&0&-\frac{L_0+2L_S}{4L_0+4L_S}&-\frac{L_0}{2L_0+2L_S}\\0&0&0&0&0\\0&0&0&0&0\\\frac{L_0}{3L_0+3L_S}&0&0&-\frac{L_0+2L_S}{6L_0+6L_S}&-\frac{L_0}{3L_0+3L_S}\\-\frac{L_0}{2L_0+2L_S}&0&0&\frac{L_0+2L_S}{4L_0+4L_S}&\frac{L_0}{2L_0+2L_S}\end{bmatrix}\\
&\times\begin{bmatrix}U_{sa}(s)\\U_{sb}(s)\\U_{sc}(s)\\U_{dc}(s)\\U_0(s)\end{bmatrix}+\begin{bmatrix}-1&0&0&0&1\\0&-1&0&0&1\\0&0&-1&0&1\\0&0&0&1&0\\0&0&0&0&0\end{bmatrix}\times\begin{bmatrix}U_{sa}(s)\\U_{sb}(s)\\U_{sc}(s)\\U_{dc}(s)\\U_0(s)\end{bmatrix}.
\end{aligned}
\tag{13}
$$

In the normal states, the controller calculates the ICVs as shown in Fig. 7, and transforms the ICVs to the arm voltage references based on (5). Considering that the single-open-arm states are just temporary abnormal states, the changing of the controller from the normal to the single-open-arm states should be as little as possible, as long as the ac- and dc-side currents can be decoupled. Therefore, this article modifies the transformation from the ICVs to the arm voltage references, while the calculation of ICVs in Fig. 7 remains. To achieve this objective, the circuit model in the single-open-arm state [i.e., Eq. (13)] must be expressed in a form similar to (4). By comparing (13) with (4), the relationship between the ICVs and the arm voltages becomes

$$
\begin{aligned}
&\begin{bmatrix}E_a(s)\\E_b(s)\\E_c(s)\\E_{dc}(s)\\E_{cirb}(s)\end{bmatrix}=\begin{bmatrix}0&0&\frac{L_0+2L_S}{2L_0+2L_S}&0&0\\-1/2&0&0&1/2&0\\0&-1/2&0&0&1/2\\\frac{1}{3}&\frac{1}{3}&\frac{L_0}{3L_0+3L_S}&\frac{1}{3}&\frac{1}{3}\\-1&\frac{1}{2}&\frac{L_0}{2L_0+2L_S}&-1&\frac{1}{2}\end{bmatrix}\\
&\times\begin{bmatrix}U_{bp}(s)\\U_{cp}(s)\\U_{an}(s)\\U_{bn}(s)\\U_{cn}(s)\end{bmatrix}+\begin{bmatrix}\frac{L_0}{2L_0+2L_S}&0&0&-\frac{L_0+2L_S}{4L_0+4L_S}&-\frac{L_0}{2L_0+2L_S}\\0&0&0&0&0\\0&0&0&0&0\\-\frac{L_0}{3L_0+3L_S}&0&0&\frac{L_0+2L_S}{6L_0+6L_S}&\frac{L_0}{3L_0+3L_S}\\-\frac{L_0}{2L_0+2L_S}&0&0&\frac{L_0+2L_S}{4L_0+4L_S}&\frac{L_0}{2L_0+2L_S}\end{bmatrix}\\
&\times\begin{bmatrix}U_{sa}(s)\\U_{sb}(s)\\U_{sc}(s)\\U_{dc}(s)\\U_0(s)\end{bmatrix}.
\end{aligned}
\tag{14}
$$

On the basis of (14), after obtaining the ICVs generated by the controllers, the arm voltage references can be obtained as

$$
\begin{aligned}
&\begin{bmatrix}U^*_{bp}(s)\\U^*_{cp}(s)\\U^*_{an}(s)\\U^*_{bn}(s)\\U^*_{cn}(s)\end{bmatrix}=\begin{bmatrix}0&-1&0&\frac{1}{2}&-\frac{1}{3}\\-\frac{L_0}{L_0+2L_S}&0&-1&1&\frac{1}{3}\\\frac{2L_0+2L_S}{L_0+2L_S}&0&0&0&0\\0&1&0&\frac{1}{2}&-\frac{1}{3}\\-\frac{L_0}{L_0+2L_S}&0&1&1&\frac{1}{3}\end{bmatrix}\times\begin{bmatrix}E_a(s)\\E_b(s)\\E_c(s)\\E_{dc}(s)\\E_{cirb}(s)\end{bmatrix}\\
&+\begin{bmatrix}0&0&0&0&0\\\frac{L_0}{L_0+2L_S}&0&0&-\frac{1}{2}&-\frac{L_0}{L_0+2L_S}\\-\frac{L_0}{L_0+2L_S}&0&0&\frac{1}{2}&\frac{L_0}{L_0+2L_S}\\0&0&0&0&0\\\frac{L_0}{L_0+2L_S}&0&0&-\frac{1}{2}&-\frac{L_0}{L_0+2L_S}\end{bmatrix}\times\begin{bmatrix}U_{sa}(s)\\U_{sb}(s)\\U_{sc}(s)\\U_{dc}(s)\\U_0(s)\end{bmatrix}.
\end{aligned}
\tag{15}
$$

Assuming that the arm voltages are equal to their references [i.e., $U_{bp}(s)=U^*{}_{bp}(s)$, $U_{cp}(s)=U^*{}_{cp}(s)$, $U_{an}(s)=U^*{}_{an}(s)$, $U_{bn}(s)=U^*{}_{bn}(s)$ and $U_{cn}(s)=U^*{}_{cn}(s)$], substituting (15) into (13) yields

$$
s\begin{bmatrix}(L_0/2+L_S)\,I_a(s)\\(L_0/2+L_S)\,I_b(s)\\(L_0/2+L_S)\,I_c(s)\\2L_0/3I_{dc}(s)\\3L_0I_{cirb}(s)\end{bmatrix}=\mathbf{C}''\times\begin{bmatrix}I^*_a(s)-I_a(s)\\I^*_b(s)-I_b(s)\\I^*_c(s)-I_c(s)\\I^*_{dc}(s)-I_{dc}(s)\\I^*_{cirb}(s)-I_{cirb}(s)\end{bmatrix}
\tag{16}
$$

where

$$
\mathbf{C}''=\begin{bmatrix}G_{ac}(s)&0&0&0&0\\0&G_{ac}(s)&0&0&0\\0&0&G_{ac}(s)&0&0\\0&0&0&G_{dc}(s)&0\\0&0&0&0&G_{cir}(s)\end{bmatrix}.
\tag{17}
$$

The matrix **C"** only contains diagonal elements, which indicates that if the controller immediately shifts the transformation from (5) to (15) once the single-open-arm states are detected, as shown in Fig. 8, the ac- and dc-side currents can be decoupled, thereby enhancing the control effects.

$$
\mathbf{C}'=\begin{bmatrix}G_{ac}(s)\frac{L_0+2L_S}{2L_0+2L_S}&0&0&-G_{dc}(s)\frac{L_0+2L_S}{4L_0+4L_S}&0\\0&G_{ac}(s)&0&0&0\\0&0&G_{ac}(s)&0&0\\-G_{ac}(s)\frac{L_0}{3L_0+3L_S}&0&0&G_{dc}(s)\frac{5L_0+4L_S}{6L_0+6L_S}&0\\G_{ac}(s)\frac{L_0}{2L_0+2L_S}&0&0&G_{dc}(s)\frac{L_0+2L_S}{4L_0+4L_S}&G_{cir}(s)\end{bmatrix}.
\tag{12}
$$

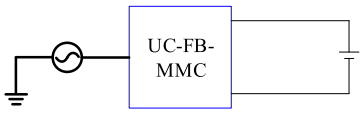

Fig. 9. Diagram of simulation and experimental models.

TABLE IV
PARAMETERS OF SIMULATIONS

Terms	Values
Rated active power / MW	1000
Rated reactive power / Mvar	±500
Rated dc voltage / kV	640
Rated dc current / kA	1.5625
Rated ac voltage / kV	506
Rated submodule voltage / kV	1.6
Quantity of submodules per arm	726
Submodule capacitance / mF	7.0
Arm inductance / mH	440

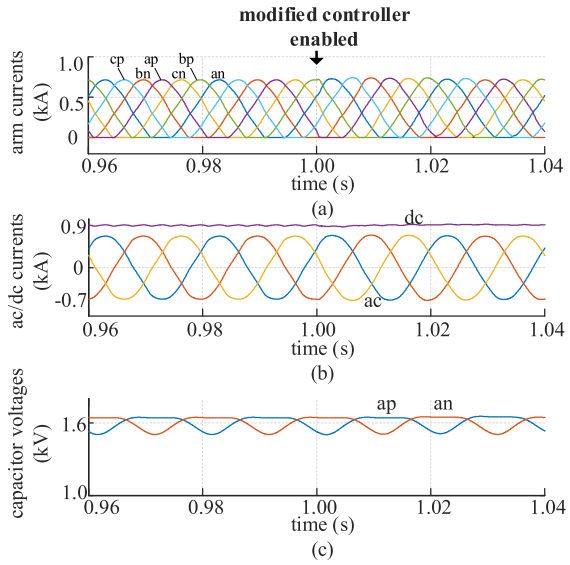

Fig. 10. Simulation results for single-open-arm states without and with the proposed modified controllers. ap and an represent the upper and lower arms of phase A, respectively.

V. SIMULATION AND EXPERIMENTAL RESULTS

A. Simulation Results

A simulation model shown in Fig. 9 was built in MATLAB/Simulink to verify the analysis and the proposed modified controller. Table IV gives the simulation parameters. The rated submodule voltage was designed as 1.6 kV. The ac voltage was designed as 506 kV to ensure unidirectional arm currents in steady states, and therefore, each converter arm consisted of 726 submodules to ensure the modulation margin.

In the first simulation, the active power was set as 600 MW. To verify the proposed theory and controller presented in Sections III and IV, the reactive power was set as 500 Mvar to create the open-arm states. Fig. 10 shows the simulation results. As shown in Fig. 10(a), the arm currents that had negative tendencies

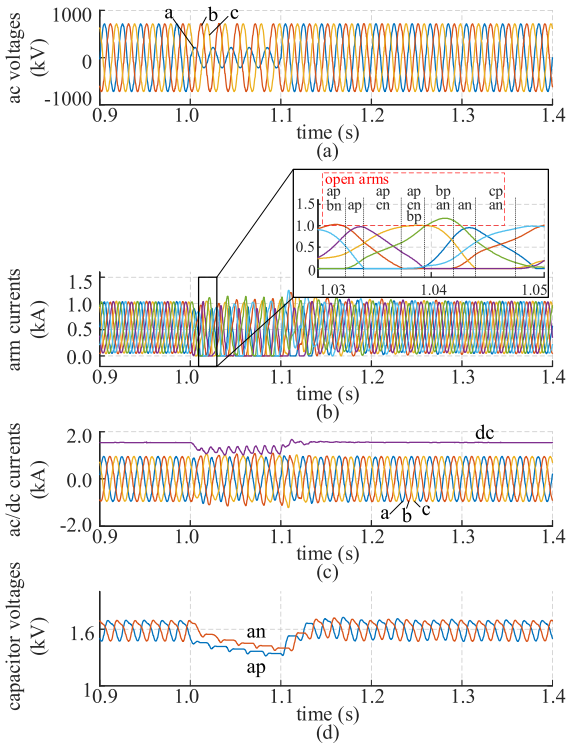

Fig. 11. Simulation results in transient open-arm states due to an AC fault.

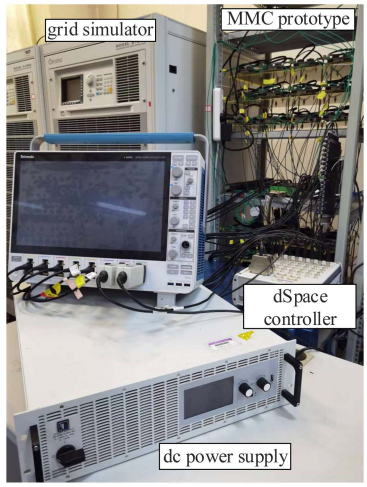

Fig. 12. Photograph of experimental platform.

TABLE V
PARAMETERS OF EXPERIMENTAL PLATFORM

Terms	Values
Rated active power / W	7000
Rated reactive power / var	±3500
Rated dc voltage / V	200
Rated dc current / A	10
Rated ac voltage / V	158
Quantity of submodules per arm	4

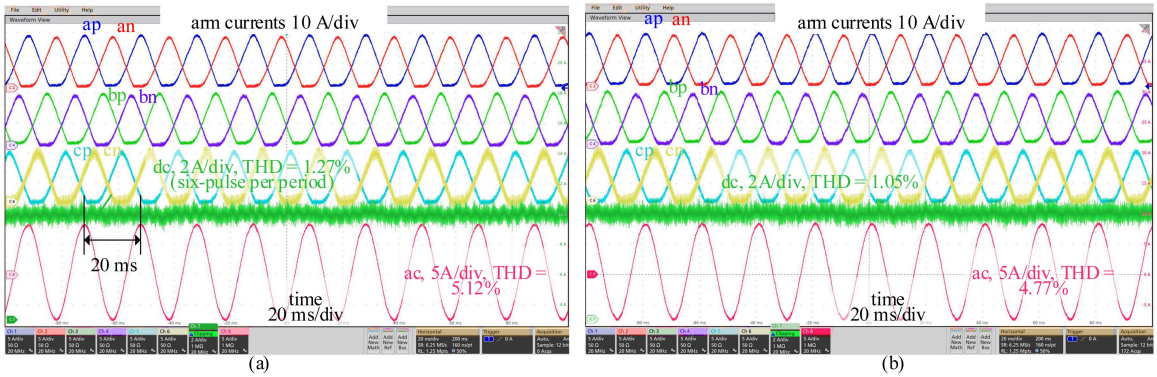

Fig. 13. Experimental results for single-open-arm states. (a) Without and (b) with the proposed modified controllers.

were clamped to 0, indicating that the UC-FB-MMC had entered the single-open-arm states, and that the open arms changed their positions among the six arms. As shown in Fig. 10(b), the ac- and dc-side currents are under control. However, some harmonics appeared in the ac- and dc-side current waveforms due to the coupling effects between ac and dc current controls. Especially, the six-pulse harmonic appeared on the dc-side current waveform. At $t = 1.0$ s, the modified controller proposed in Section IV was enabled to decouple the ac and dc current controls. Clearly, in Fig. 10(b), the ripples on the dc-side currents and the harmonics in the ac-side currents disappeared. Moreover, the effectiveness of the modified controller can also verify the mathematical model deduced in Section III.

The transient state caused by an ac fault was simulated, and Fig. 11 shows the results. Before the fault occurred, the UC-FB-MMC was transmitting active power of 1000 MW and reactive powers of 500 Mvar in the steady state. A single phase-to-ground fault was simulated from $t = 1.0$ to 1.1 s. During the fault, the voltage of phase A decreased to 0.3 p.u. Given that the ac- and dc-side currents were affected, the positive arm currents were disrupted. As shown and zoomed in Fig. 11(b), the arm currents that had negative tendencies were clamped to 0, indicating that the UC-FB-MMC entered the single-, double- and triple-open-arm states. During the open-arm states, at least three converter arms were operating, which verifies that the ac- and dc-side current paths still existed, and that the ac- and dc-side currents could still flow, as shown in Fig. 11(c). After $t = 1.1$ s, when the fault was cleared, the UC-FB-MMC quickly returned to the normal state with all the arm currents positive. The simulation results shown in Fig. 11 verify the analysis in Section II. First, at least three converter arms in a UC-FB-MMC have positive arm currents and are in operation. Second, even if some converter arms cannot guarantee positive currents, the ac- and dc-side currents can continue flowing, and the operation of the converter is not interrupted.

B. Experimental Results

An experimental platform was built to verify the analysis. Fig. 9 shows the diagram, Fig. 12 shows the photograph, and Table V shows the parameters. The down-scaled experimental

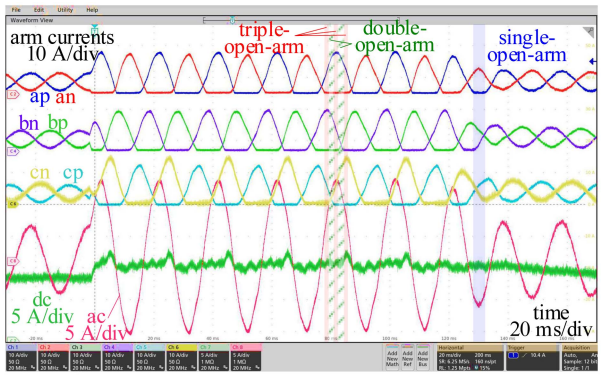

Fig. 14. Experimental results in transient open-arm states.

platform has the same structure and control strategies as the MW-level MMC converters. Therefore, the operation characteristics in the open-arm states of the MW-level UC-FB-MMCs can be reflected using the down-scaled experimental platform.

The experiments of single-open-arm states were conducted. The active power was 2000 W, and the reactive power was 1500 var, thereby creating the single-open-arm states. Fig. 13(a) and (b) shows the results without and with the proposed modified controllers, respectively. The results in Fig. 13(a) indicate that the UC-FB-MMC could operate in the single-open-arm state, and that the ac- and dc-side currents were under control. However, the current control effects were affected by the coupling effects. Especially, because the open arm changed its position in the six converter arms, the six-pulse harmonic appeared on the dc-side current waveform. By contrast, Fig. 13(b) shows the results when implementing the modified controller. Although there were still some harmonics because each converter arm only contained four submodules, the six-pulse harmonic were eliminated from the dc-side current waveform, and the total harmonic distortion (THD) was reduced from 1.27% to 1.05%. In the ac-side current waveform, the THD was also reduced from 5.12% to 4.77%. The effectiveness of the proposed modified controller can also verify the mathematical model deduced in Section III.

A transient experiment of the open-arm states was conducted, and Fig. 14 shows the results. In the normal state, the MMC was

operating with 2000 W active power and 0 reactive power. The reactive power reference was increased to 3500 var for 100 ms and then back to 0 to create the transient open-arm states. As marked in Fig. 14, the single-, double- and triple-open-arm states appeared. During the transient state, at least three arms were in operation, and thus, the ac- and dc-side currents were not interrupted, thereby verifying the analysis and supporting the conclusion in Section II.

VI. Conclusion

This article conducts research on the operation characteristics of the UC-FB-MMC with non-positive arm currents. The current path analysis is conducted first. The result indicates that if an arm current reaches zero and tends to be negative in a transient state, then it is clamped to approximately 0, and thus, the converter arm becomes approximately equivalent to an open circuit. On this basis, the concepts of single-, double- and triple-open-arm states are proposed. In all these conditions, the ac- and dc-side current paths still exist, and the ac- and dc-side currents will not be interrupted. Therefore, over voltage due to sudden interruption of the currents will not occur. Subsequently, the single-open-arm state is taken as an example, and the mathematical model of the UC-FB-MMC is deduced. The result verifies that the ac- and dc-side currents are still under control, but the control effect becomes poor. After that, a modified controller that can enhance the current control effects during the single-open-arm states is presented. The simulation and experimental results verify the analysis.

References

[1] A. Lesnicar and R. Marquardt, "An innovative modular multilevel converter topology suitable for a wide power range," in *Proc. IEEE Bologna Power Tech Conf. Proc.*, 2003, vol. 3, pp. 6–11, doi: 10.1109/PTC.2003.1304403.

[2] R. Marquardt, "Modular multilevel converter: An universal concept for HVDC-networks and extended DC-bus-applications," in *Proc. Int. Power Electron. Conf. - ECCE ASIA*, 2010, pp. 502–507.

[3] H. Rao et al., "Key technologies of ultra-high voltage hybrid LCC-VSC MTDC systems," *CSEE J. Power Energy Syst.*, vol. 5, no. 3, pp. 365–373, Sep. 2019.

[4] G. Guo et al., "HB and FB MMC based onshore converter in series-connected offshore wind farm," *IEEE Trans. Power Electron.*, vol. 35, no. 3, pp. 2646–2658, Mar. 2020, doi: 10.1109/TPEL.2019.2929689.

[5] Z. Li, Q. Song, R. Zeng, B. Zhao, J. Meng, and Z. Deng, "A DC grid access solution based on series-connected distributed full-bridge submodule-based MMCs," in *Proc. IEEE 28th Int. Symp. Ind. Electron.*, 2019, pp. 697–701, doi: 10.1109/ISIE.2019.8781208.

[6] V. Hussennether, J. Rittiger, A. Barth, and D. Worthington, "Projects BorWin2 and HelWin1 – Large scale multilevel voltage-sourced converter technology for bundling of offshore windpower," 2012.

[7] J. Hu, Z. He, L. Lin, K. Xu, and Y. Qiu, "Voltage polarity reversing-based DC short circuit FRT strategy for symmetrical bipolar FBSM-MMC HVDC System," *IEEE J. Emerg. Sel. Topics Power Electron.*, vol. 6, no. 3, pp. 1008–1020, Sep. 2018, doi: 10.1109/JESTPE.2018.2820076.

[8] Q. Song, S. Xu, Y. Zhou, Y. Gim, Z. Li, and Z. Deng, "Active fault-clearing on long-distance overhead lines using a hybrid modular multilevel converter," in *Proc. IEEE 28th Int. Symp. Ind. Electron.*, 2019, pp. 2033–2038, doi: 10.1109/ISIE.2019.8781312.

[9] G. Li et al., "Power reversal strategies for hybrid LCC/MMC HVDC systems," *CSEE J. Power Energy Syst.*, vol. 6, no. 1, pp. 203–212, Mar. 2020.

[10] W. Lin, D. Jovcic, S. Nguefeu, and H. Saad, "Full-bridge MMC converter optimal design to HVDC operational requirements," *IEEE Trans. Power Del.*, vol. 31, no. 3, pp. 1342–1350, Jun. 2016, doi: 10.1109/TPWRD.2015.2475130.

[11] Y. Lyu, C. Li, Y. Hsieh, F. C. Lee, Q. Li, and R. Xu, "Capacitor voltage ripple reduction with state trajectory analysis for modular multilevel converter," in *Proc. IEEE Appl. Power Electron. Conf. Expo.*, 2017, pp. 1829–1836, doi: 10.1109/APEC.2017.7930947.

[12] Q. Song, W. Yang, B. Zhao, S. Xu, H. Rao, and Z. Zhu, "Energy storage requirement reduction using negative-voltage states of a full-bridge modular multilevel converter," *IEEE Trans. Power Electron.*, vol. 34, no. 6, pp. 5243–5255, Jun. 2019, doi: 10.1109/tpel.2018.2869464.

[13] G. J. M. d. Sousa and M. L. Heldwein, "Modular multilevel converter based unidirectional medium/high voltage drive system," in *Proc. IEEE 39th Annu. Conf. Ind. Electron. Soc.*, 2013, pp. 1037–1042, doi: 10.1109/IECON.2013.6699276.

[14] G. J. M. d. Sousa and M. L. Heldwein, "Three-phase unidirectional modular multilevel converter," in *Proc. 15th Eur. Conf. Power Electron. Appl.*, 2013, pp. 1–10.

[15] X. Yu, Y. Wei, and Q. Jiang, "New submodule circuits for modular multilevel current source converters with DC fault ride through capability," in *Proc. IEEE Appl. Power Electron. Conf. Expo.*, 2016, pp. 1468–1474, doi: 10.1109/APEC.2016.7468062.

[16] W. Yang, Q. Song, S. Xu, H. Rao, and W. Liu, "An MMC topology based on unidirectional current H-Bridge submodule with active circulating current injection," *IEEE Trans. Power Electron.*, vol. 33, no. 5, pp. 3870–3883, May 2018, doi: 10.1109/tpel.2017.2722011.

[17] Z. Deng, D. Chen, N. Mei, W. Yang, Z. Li, and Q. Song, "The control strategy of unidirectional current H-Bridge MMC based Hybrid HVDC system," in *Proc. IEEE 28th Int. Symp. Ind. Electron.*, 2019, pp. 2070–2075, doi: 10.1109/ISIE.2019.8781215.

[18] Z. Li et al., "Energy diverting converter topology using unidirectional current H-bridge submodules for VSC-HVDC transmission system," *IEEE Trans. Power Electron.*, vol. 37, no. 5, pp. 5299–5308, May 2022, doi: 10.1109/TPEL.2021.3133498.

[19] Z. Li et al., "Low-cost and compact asymmetrical unidirectional-current modular multilevel converters," *IEEE Trans. Power Electron.*, vol. 38, no. 3, pp. 3398–3411, Mar. 2023, doi: 10.1109/TPEL.2022.3225861.

[20] W. Yang, Q. Song, and B. Zhao, "Energy storage requirement and low capacitance operation of unidirectional current H-Bridge modular multilevel converters," *IEEE Trans. Power Electron.*, vol. 34, no. 12, pp. 11748–11759, Dec. 2019, doi: 10.1109/TPEL.2019.2910456.

[21] W. Yang, Q. Song, and W. Liu, "Decoupled control of modular multilevel converter based on intermediate controllable voltages," *IEEE Trans. Ind. Electron.*, vol. 63, no. 8, pp. 4695–4706, Aug. 2016, doi: 10.1109/TIE.2016.2549001.

[22] J. Wang and P. Wang, "Decoupled power control for direct-modulation-based modular multilevel converter with improved stability," *IEEE Trans. Ind. Electron.*, vol. 66, no. 7, pp. 5264–5274, Jul. 2019, doi: 10.1109/tie.2018.2870352.

Zhengxuan Li was born in Beijing, China, in 1995. He received the B.S. degree in electrical engineering from the School of Electrical and Electronic Engineering, North China Electric Power University, Beijing, China, in 2018, and the Ph.D. degree in electrical engineering from the Department of Electrical Engineering, Tsinghua University, Beijing, China, in 2023.

He is currently a Postdoctoral Fellow with Tsinghua University, Beijing, China. His current research interest includes modular multilevel converter, wind power and VSC-HVDC transmission system.

Qiang Song (Senior Member, IEEE) was born in Changchun, China, in 1975. He received the B.E.E. and Ph.D. degrees from Tsinghua University, Beijing, China, in 1998 and 2003, respectively, both in electrical engineering.

From 2003 to 2008, he was a Lecturer with the Department of Electrical Engineering, Tsinghua University. Since 2008, he has been an Associate Professor with the Department of Electrical Engineering, Tsinghua University. His main research interests include high power electronic interfaces for utility system, flexible ac transmission system, VSC-HVDC system, and custom power quality.

Biao Zhao (Senior Member, IEEE) was born in Hubei, China, in 1987. He received the B.S. degree in electrical engineering from the Department of Electrical Engineering, Dalian University of Technology, Dalian, China, in 2009, and the Ph.D. degree in electrical engineering from the Department of Electrical Engineering, Tsinghua University, Beijing, China, in 2014.

He is currently an Associate Professor with the Department of Electrical Engineering, Tsinghua University, Beijing, China. His research interests include high power converters, high power semiconductor devices, and flexible dc transmission and distribution systems.

Dr. Zhao is a Senior Member of the Chinese Society for Electrical Engineering and the Chinese Electro-Technical Society.

Zhanqing Yu (Member, IEEE) was born in Inner Mongolia, China, in 1981. He received the B.Sc. and Ph.D. degrees in electrical engineering from the Department of Electrical Engineering, Tsinghua University, Beijing, China, in 2003 and 2008, respectively.

After graduation, in 2008 and 2010, he was a Post Doctor and a Lecturer with the Department of Electrical Engineering, Tsinghua University, Beijing, China, he was an Associate Professor with the same department in 2012. He has participated in several projects sponsored by High-Tech R&D Program (863 Program), National Basic Research Program of China (973 Program), National Natural Science Foundation of China. His research interests include dc grid, dc breaker, electromagnetic environment and electromagnetic compatibility, lightning protection.

Rong Zeng (Senior Member, IEEE) was born in Shaanxi, China, in 1971. He received the B.Eng., M.Eng., and Ph.D. degrees from the Department of Electrical Engineering, Tsinghua University, Beijing, China, in 1995, 1997, and 1999, respectively.

In 1999, he was a Lecturer with the Department of Electrical Engineering, Tsinghua University, where he was an Associate Professor and a Professor with the same department in 2002 and 2007, respectively. He is currently working in the fields of air gap discharge, lightning protection, and electromagnetic compatibility in power systems, electric and magnetic field measurement by integrated electro-optical sensors, power semiconductor, HVDC system and direct current circuit breaker.

Bin Cui (Member, IEEE) was born in Jinan, China, in 1987. He received the B.S. degree in electrical engineering from Harbin Institute of Technology (HIT), Harbin, China, in 2009, the M.S. degree in electrical engineering from Fuzhou University, Fuzhou, China, in 2012, and the Ph.D. degree from the Department of Electrical Engineering, Tsinghua University, Beijing, China, in 2019.

He is currently an Associate Research Fellow with the State Key Laboratory of Power System Operation and Control, Tsinghua University. His research interest includes high frequency dc–dc converters, high frequency transformers, high power converter, and flexible dc transmission and distribution system.